

# Zr<sub>6</sub>Ni<sub>6</sub>TiSiO<sub>x</sub>: A New Structure Type with a Mixed Early-Late Transition-Metal Framework

Richard Mackay and H. F. Franzen\*

Iowa State University, Department of Chemistry and Ames Lab—DOE,<sup>1</sup> Ames, Iowa 50011

Received February 2, 1993. Revised Manuscript Received April 5, 1993

An interstitially stabilized intermetallic in a mixed early-late transition-metal system has been found to crystallize in a new structure type. The new compound Zr<sub>6</sub>Ni<sub>6</sub>TiSiO<sub>x</sub> ( $x = 1.8$ ) was synthesized by melting Zr, Ni, Si, and Ti<sub>2</sub>O<sub>3</sub> in an arc furnace, followed by annealing in vacuum at 900–1150 °C. The crystal structure was determined by refinement of single-crystal X-ray diffraction data. The structure was refined in the centrosymmetric space group  $P\bar{3}m1$ ,  $Z = 2$ , with lattice parameters  $a = b = 8.2778(9)$  Å, and  $c = 7.444(1)$  Å ( $R = 0.030$ ,  $R_w = 0.033$ ). Oxygen atoms center zirconium trigonal antiprisms, which share faces to form a three-dimensional network. The titanium and silicon atoms are coordinated by icosahedra of nickel or of zirconium and nickel atoms. A structural comparison with the  $\kappa$ -phase will be discussed.

## Introduction

A substantial diversity of structures of binary compounds in mixed early-late transition-metal systems, particularly in the Zr–Ni system, is described in the literature.<sup>2,3</sup> Typically, when an interstitial element reacts with a binary early-late transition-metal compound to form a ternary compound, the compound crystallizes in a common structure type. In fact, only a limited number of structure types are known for phases of mixed early and late transition metals which are interstitially stabilized.<sup>4</sup> Recent work in this lab has investigated the importance of the presence of small amounts of oxygen in stabilizing phases in the Zr–Ni system which do not appear as true binary intermetallic compounds (i.e., the cubic Laves phase,<sup>2–5</sup> the filled Ti<sub>2</sub>Ni type structure,<sup>6</sup> and the filled Re<sub>3</sub>B type structure<sup>7–9</sup>).

The ternary metal system Zr–Ti–Ni contains phases which do not occur in either of the binary systems Zr–Ni or Ti–Ni (i.e., the hexagonal Laves phase ZrTiNi<sup>10,11</sup> and the BaPb<sub>3</sub> type structure ZrTi<sub>2</sub>Ni<sub>9</sub><sup>12,13</sup>). It is natural to expect that interstitials in this ternary system may stabilize new compounds, with respect to the ternary intermetallics and interstitially stabilized binary compounds. There are some examples of ternary and quaternary phases which

form with the addition of an interstitial atom, such as oxygen in the case of a few  $\kappa$ -phases (e.g., Zr<sub>3</sub>W<sub>4</sub>(S,Ni)O<sub>3</sub>).<sup>14–16</sup> Now, a new interstitially stabilized compound has been formed in the Zr–Ti–Ni system with the composition Zr<sub>6</sub>Ni<sub>6</sub>TiSiO<sub>1.8</sub>. Reported here are the structural results of a single crystal refinement, and a comparison of this structure with the  $\kappa$ -phase structure.

## Experimental Section

Samples were prepared from mixtures of Zr (Alfa products, 0.25-mm foil, 99.9%), Ti (Ames Lab), Ni (Inco, 99.99%), (Johnson Matthey, zone refined, 99.999%), and Ti<sub>2</sub>O<sub>3</sub> (Johnson Matthey, 99+%). The metal pieces were treated in acid solutions to remove surface oxides and sequentially rinsed in water and then methanol. The zirconium cleaning solution was a mixture of 10% HF, 45% HNO<sub>3</sub>, and 45% H<sub>2</sub>O by volume. Titanium was cleaned in a solution of 60% H<sub>2</sub>O<sub>2</sub> (30%), 10% HF, and 30% H<sub>2</sub>O by volume. Nickel was cleaned in concentrated HNO<sub>3</sub>.

All samples were arc melted three times on a water-cooled copper plate with a thoriated nonconsumable tungsten electrode in an argon atmosphere. The arc melted buttons were subsequently crushed and pressed into pellets and annealed in evacuated silica tubes at 900–1150 °C for 2–3 days. All samples contained ZrO<sub>2</sub> as a minor phase.

The single crystal used for the structural investigation was picked from a sample of a Zr–Ti–Ni alloy which was accidentally melted and reacted with the silica tube in the annealing process. Subsequent reactions included silicon and oxygen in the starting materials. All handling of materials was done in air.

X-ray powder diffraction techniques were used to identify the phases present and to determine accurate lattice parameters. Powder diffraction films were obtained using a vacuum Guinier camera FR552 (Enraf-Nonius, Delft, the Netherlands) with Cu K $\alpha_1$  radiation. Lattice parameters were determined by a least-squares refinement of indexed line positions calibrated by an internal silicon standard (NIST).

Single-crystal X-ray diffraction data collection was done on a Rigaku AFC6R diffractometer. The structure was solved by direct methods and refined using the SHELXS<sup>17</sup> and TEXSAN<sup>18</sup> software packages. Details of crystal data are listed in Table I.

(1) The Ames Laboratory—DOE is operated for the U.S. Department of Energy by Iowa State University under Contract No. W-7405-Eng-82. This research was supported by the Office of the Basic Energy Sciences, Materials Sciences Division.

(2) Bsenko, L. J. *Less-Common Met* 1979, 63, 171.

(3) Kirkpatrick, M. E.; Larsen, W. L. *Trans. Am. Soc. Met.* 1961, 54, 580.

(4) Leonard, S. R.; Snyder, B. S.; Brewer, L.; Stacy, A. M. *J. Solid State Chem.* 1991, 92, 39.

(5) Petkov, V. V.; Markiv, V. Ya.; Gorskiy, V. V. *Russ. Metallurgy* 1972, 2, 188.

(6) Mackay, R.; Franzen, H. F., unpublished results.

(7) Mackay, R.; Franzen, H. F. *J. Alloys Compounds* 1992, 186, L7.

(8) Nevitt, M. V.; Downey, J. W. *Trans. Met. Soc. AIME* 1961, 221, 1014.

(9) Boller, H. *Monatsh. Chem.* 1973, 104, 545.

(10) Semenenko, K. N.; Verbetskii, V. N.; Mitrokhin, S. V.; Burnasheva, V. V. *Russ. J. Inorg. Chem.* 1980, 25, 961.

(11) Molokanov, V. V.; Chebotnikov, V. N.; Kovneristiy, Yu. K. *Inorg. Mater.* 1989, 25, 46.

(12) van Vucht, J. H. N. *J. Less-Common Met.* 1966, 11, 308.

(13) Glimois, J. L.; Forey, P.; Guillen, R.; Feron, J. L. *J. Less-Common Met.* 1987, 134, 221.

(14) Mackay, R.; Franzen, H. F. *Z. Anorg. Allg. Chem.* 1992, 616, 154.

(15) Hårsta, A. *J. Solid State Chem.* 1985, 57, 373.

(16) Hårsta, A.; Rundqvist, S. *J. Solid State Chem.* 1987, 70, 210.

(17) Sheldrick, G. M. In *Crystallographic Computing*; Sheldrick, G. M., Krüger, C., Goddard, R., Eds.; Oxford University Press: Oxford, 1985; Vol. 3, pp 175–189.

Table I. Crystal Data for  $\text{Zr}_6\text{Ni}_6\text{TiSiO}_x$ 

formula	$\text{Zr}_{5.39}\text{Ni}_{6.00}\text{Ti}_{1.71}\text{Si}_{0.90}\text{O}_{1.80}$
space group	$P\bar{3}m1(164)$
$a$ , Å	8.2778(9)
$c$ , Å	7.444(1)
$V$ , Å <sup>3</sup>	441.7(1)
$Z$	2
$d_{\text{calc}}$ , g/cm <sup>3</sup>	7.366
crystal size, mm <sup>3</sup>	$0.08 \times 0.04 \times 0.04$
$\mu$ (Mo K $\alpha$ ), cm <sup>-1</sup>	200.84
data collection instrument	Rigaku AFC6R
radiation (monochromated in incident beam)	Mo K $\alpha$ ( $\lambda = 0.71069$ Å)
temperature, °C	$23 \pm 1$
scan method	$2\theta-\omega$
octants measured	$\pm h \pm k l$
data collection range $2\theta$ , deg	0–60
no. reflns measured	2897
no. unique data, total with $F_o^2 > 3\sigma(F_o^2)$	272
no. parameters refined	37
trans factors, max/min	1.500
secondary extinction coefficient	$2.0(8) \times 10^{-7}$
$R$ , <sup>a</sup> $R_w$ , <sup>b</sup> GOF <sup>c</sup>	0.030, 0.033, 1.006
largest peak, e/Å <sup>3</sup>	1.44
largest negative peak, e/Å <sup>3</sup>	-1.89

<sup>a</sup>  $R = \sum |F_o| - |F_c| / \sum |F_o|$ . <sup>b</sup>  $R_w = [\sum w(|F_o| - |F_c|)^2 / \sum w|F_o|^2]^{1/2}$ ;  $w = 1/\sigma^2(|F_o|)$ . <sup>c</sup>  $\text{GOF} = \sum (|F_o| - |F_c|)^2 / (N_{\text{obs}} - N_{\text{parameters}})$ .

Table II. Positional Parameters for  $\text{Zr}_6\text{Ni}_6\text{TiSiO}_x$ <sup>a</sup>

atom	$x$	$y$	$z$	$B(\text{eq})$	% occup
Ni(1)	0.1129(2)	-0.1129	0.2553(3)	0.54(2)	100
Ni(2)	0.1726(2)	-0.1726	0.9326(3)	0.54(2)	100
Zr(1)	0.4598(1)	-0.4598	0.1953(2)	0.63(2)	100
Zr(2)					79(2)
Ti	0.2073(1)	-0.2073	0.5688(2)	0.49(3)	21(2)
Ti(1)	0	0	0	0.4(2)	100
Ti(2)	0	0	$1/2$	0.7(2)	100
Si					90(4)
Ti	$1/3$	$2/3$	0.874(1)	0.4(2)	10(4)
O(1)	$1/2$	0	$1/2$	0.7(3)	96(4)
O(2)	$1/3$	$2/3$	0.367(9)	0.4(8)	36(6)

<sup>a</sup>  $B(\text{eq}) = (8\pi^2/3) \sum_{i=1}^3 \sum_{j=1}^3 U_{ij} a_i^* a_j^* \hat{a}_i^* \hat{a}_j^*$ .

Semiquantitative analysis by energy-dispersive X-ray analysis (EDX) was carried out on a Cambridge S-200 scanning electron microscope with a Northern Tracor Micro Z-II X-ray detector. Surface analysis by X-ray photoelectron spectroscopy was performed on a Perkin-Elmer 5500 multitechnique system.

A Quantum Design SQUID magnetometer was used to check for superconductivity and to measure magnetic behavior at a field of 3 T over the temperature range 6–298 K.

## Results

The crystal was found to exhibit Laue symmetry  $\bar{3}m1$ , and the single-crystal refinement was carried out in the centrosymmetric space group  $P\bar{3}m1$ . The refinement converged with the placement of the Zr, Ni, Ti, Si and O(1) atoms at the proper sites. The refinement improved significantly when titanium was allowed to partially occupy the Zr(2) position and also to partially occupy the Si position. At this point, a peak in the Fourier difference map suggested the presence of another oxygen atom, O(2). This atom was added to the refinement, and the multiplicities of both oxygen atoms were allowed to vary. The final positional parameters, equivalent  $B$  values, and occupancies of all sites are listed in Table II. The refinement reported here was calculated using a  $F_o^2 > 3\sigma(F_o^2)$  cutoff. An additional refinement using a  $1\sigma$  cutoff

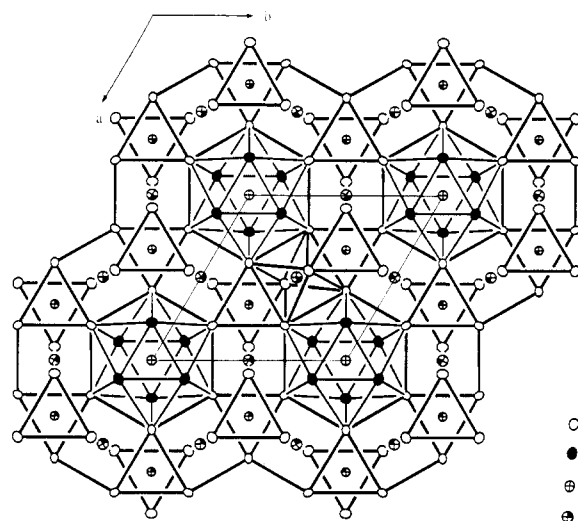


Figure 1. Projection of layer A, showing atoms at positions with  $z = 1/2 \pm 0.33$  (Ni(2), Ti(1), and Si not in this layer). Zr trigonal antiprism outlined at cell center.

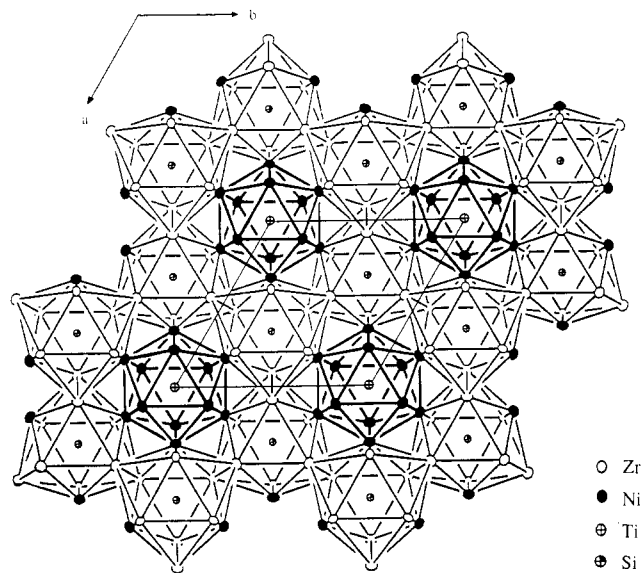
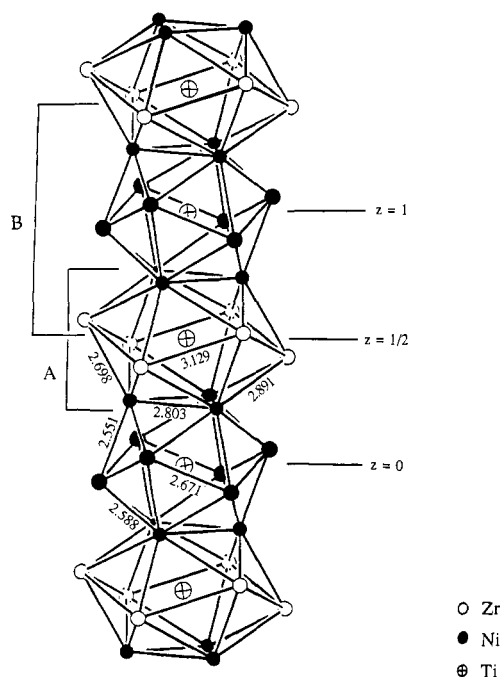


Figure 2. Projection of layer B, showing atoms at positions with  $-1/2 < z < 1/2$  (O(1), O(2), and Ti(2) at  $z = 1/2$  not in this layer).

resulted in  $R = 0.054$  and  $R_w = 0.043$  and no significant change in the thermal or positional parameters. The anisotropic thermal parameters of all non-oxygen atoms and structure factor tables including unobserved reflections are available in the supplementary material (see paragraph at end of paper).

The structure can be described by viewing two connected, alternating layers, the projections of which are shown in Figures 1 and 2. The layers are labeled A and B, as shown in Figure 3. Figure 1 shows layer A, centered at  $z = 1/2$  and containing only the atoms within the range  $z = 1/2 \pm 1/3$ . This layer consists of a network of face-sharing zirconium trigonal antiprisms which form buckled rings. The bold lines mark the Zr–Zr connections that outline the rings. Titanium atoms in an icosahedral environment are in the center of the rings. A common feature in oxygen-stabilized intermetallics of zirconium is the presence of oxygen in the center of the zirconium trigonal antiprisms. The antiprisms in the buckled ring are centered by oxygen in two distinct crystallographic sites, one of which (O(2)) is only approximately one-third



**Figure 3.** View along the *c* axis. Icosahedral coordination of Ti atoms shown. Side view of regions included in layers A and B, which are shown in projection in Figures 1 and 2, respectively.

occupied (this is the antiprism with the 3-fold axis along the *c* axis, as viewed in the projection in Figure 1). The antiprisms in the ring, then, form an alternating pattern of filled, and partially filled antiprisms. The Zr–O distances (2.22–2.35 Å) are typical of oxygen-centered zirconium antiprisms in intermetallic compounds ( $d_{\text{Zr-O}} = 2.305\text{--}2.307$  Å in Zr<sub>3</sub>NiO<sup>7</sup> and 2.27 Å in Zr<sub>4</sub>Ni<sub>2</sub>O<sup>6</sup>). The short O(1)–O(2) distance (2.59 Å) suggests full occupancy of both sites would be energetically unfavorable, similar to the situation of filling adjacent octahedral sites in the Ti<sub>2</sub>Ni type structures.<sup>19</sup> The icosahedron around the titanium atom consists of six zirconium and six nickel atoms. Distances in the Ni<sub>6</sub>Zr<sub>6</sub> icosahedron are indicated in Figure 3. Figure 4 shows the distances within the zirconium network. All interatomic distances less than 3.6 Å are listed in Table III.

Figure 2 shows the projection along *c* of layer B, centered at *z* = 0 and including all atoms except those at *z* = ±1/2. The bold outlines show the Ni<sub>12</sub> icosahedra, centered by titanium at the unit cell origin. Figure 3 illustrates how this Ni<sub>12</sub> icosahedron shares faces and stacks with the Ni<sub>6</sub>–Zr<sub>6</sub> icosahedron centered at *z* = 1/2. The Ni<sub>12</sub> unit is a fairly regular icosahedron, with a slight expansion at the top and bottom ( $d_{\text{Ni}_1\text{--Ni}_1} = 2.80$  Å, compared to  $d_{\text{Ni}_1\text{--Ni}_2} = 2.55$  Å or  $d_{\text{Ni}_2\text{--Ni}_2} = 2.67$  Å). This expansion is necessary to allow face-sharing chains to form with the larger and more irregular Ni<sub>6</sub>Zr<sub>6</sub> icosahedron. The central titanium atom has very short titanium–nickel distances in all of these icosahedron (2.44–2.52 Å). They are shorter, in fact, than any of the nickel–nickel distances (2.55–2.80 Å). A calculation of Pauling bond orders<sup>20</sup> was carried out on this compound, and the short distances and high coordination give the titanium atoms an unusually high bond order in comparison to the other transition metal atoms.

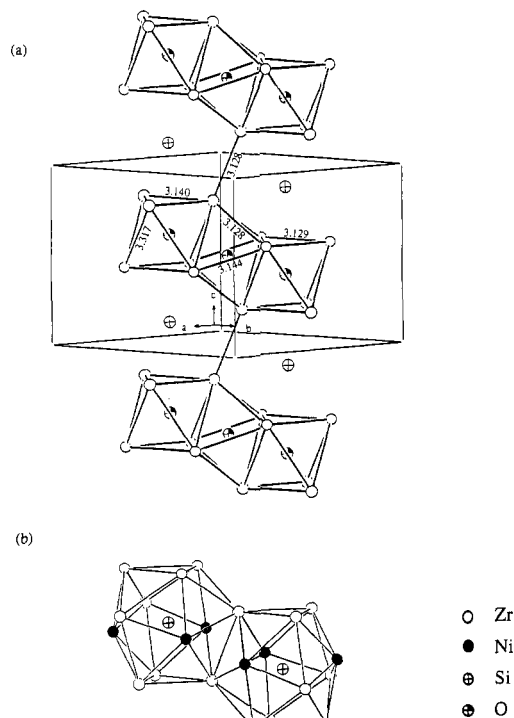


**Figure 4.** (a) Zr–Zr distances within and between layers of face-sharing trigonal antiprisms. (b) Two edge-sharing silicon-centered icosahedra, which lie between the zirconium layers in (a).

**Table III.** Interatomic Distances in Zr<sub>6</sub>Ni<sub>6</sub>TiSiO<sub>x</sub> (Å) (Distances Less Than 3.6 Å Listed)

Ni(1)–Ti(2)	2.436(2) × 1	Ni(2)–Si	2.345(2) × 1
Ti(1)	2.496(2) × 1	Ti(1)	2.525(2) × 1
Ni(2)	2.551(3) × 1	Ni(1)	2.551(3) × 1
Ni(2)	2.588(2) × 2	Ni(1)	2.588(2) × 2
Zr(2)	2.698(2) × 1	Ni(2)	2.671(2) × 2
Zr(1)	2.784(2) × 2	Zr(2)	2.754(2) × 1
Ni(1)	2.803(3) × 2	Zr(1)	2.860(1) × 2
Zr(2)	2.891(2) × 2	Zr(1)	2.871(2) × 2
O(2)	3.27(4) × 1	Zr(2)–O(1)	2.2179(6) × 2
O(1)	3.386(1) × 2	O(2)	2.35(4) × 1
Zr(1)–O(2)	2.22(4) × 1	Ni(1)	2.698(2) × 1
O(1)	2.340(1) × 1	Ni(2)	2.754(2) × 1
Ni(1)	2.784(2) × 2	Ni(1)	2.891(2) × 2
Ni(2)	2.860(1) × 2	Si	2.903(6) × 1
Ni(2)	2.871(2) × 2	Ti(2)	3.017(2) × 1
Si	3.001(6) × 1	Zr(1)	3.128(2) × 2
Si	3.011(2) × 1	Zr(2)	3.129(3) × 2
Zr(1)	3.128(3) × 1	Zr(2)	3.144(2) × 2
Zr(2)	3.128(2) × 2	Zr(1)	3.317(2) × 2
Zr(1)	3.140(3) × 2	Ti(2)–Ni(1)	2.436(2) × 6
Zr(2)	3.317(2) × 2	Zr(2)	3.017(2) × 6
Ti(1)–Ni(1)	2.496(2) × 6	O(1)–Zr(2)	2.2179(6) × 4
Ni(2)	2.525(2) × 6	Zr(1)	2.340(1) × 2
Si–Ni(2)	2.345(2) × 3	O(2)	2.52(2) × 2
Zr(2)	2.903(6) × 3	Ni(1)	3.386(1) × 4
Zr(1)	3.001(6) × 3	O(2)–Zr(1)	2.22(4) × 3
Zr(1)	3.011(2) × 3	Zr(2)	2.35(4) × 3
		O(1)	2.52(2) × 3
		Ni(1)	3.27(4) × 3

This short titanium–nickel distance, however, was also observed in Ti<sub>2</sub>Ni and the filled-Ti<sub>2</sub>Ni, Ti<sub>4</sub>Ni<sub>2</sub>O, structures ( $d_{\text{Ti-Ni}} = 2.48$  and 2.46 Å, respectively), in which Ti also centers Ni<sub>12</sub> icosahedra.<sup>21</sup>

The projection in Figure 2 shows a Ni<sub>12</sub> icosahedron sharing six vertices with six very distorted silicon-centered

(19) Newsam, J. M.; Jacobson, A. J.; McCandlish, L. E.; Polizzotti, R. *S. J. Solid State Chem.* 1988, 75, 296.

(20) Pauling, L. *The Nature of the Chemical Bond*, 3rd ed.; Cornell University Press: Ithaca, NY, 1948.

(21) Mueller, H. M. H.; Knott, H. W. *Trans. Met. Soc. AIME* 1963, 227, 674.

icosahedra. The distortion is seen in the very short Si-Ni distances (2.34 Å), compared with the Si-Zr distances (2.90–3.01 Å). These silicon-centered icosahedra form a network of edge-sharing icosahedra. Figure 4b shows how two of these icosahedra share edges. Figure 4a shows the location of the silicon in between the layers of zirconium antiprisms. The trigonal antiprisms and icosahedra share faces. Thus, the structure consists of a metal framework of zirconium trigonal antiprisms and nickel icosahedra which arrange in this three-dimensional network. Titanium and silicon fill the icosahedral sites, and oxygen occupies trigonal antiprismatic sites.

The crystal structure refinement yields the atomic ratios Ni:Zr:Ti:Si of 6:5.4:1.7:0.9, to be compared with the idealized atomic ratios of 6:6:1:1. A small piece of the sample from which the crystal was extracted was studied by both EDX and XPS techniques. Surface analysis on a sample which was ion-beam etched in an argon atmosphere gave ratios of 6:5.8:1.6:0.5. Semiquantitative elemental analysis by EDX on a rough surface also resulted in a Ni:Zr ratio greater than 1, with excess titanium, supporting the conclusion that titanium substitutes on the zirconium sites. The EDX experiment did not, however, indicate a deficiency in silicon. A bulk sample prepared with starting stoichiometry  $\text{Zr}_6\text{Ni}_6\text{TiSiO}_2$ , and containing both the desired phase and  $\text{ZrO}_2$ , had lattice parameters  $a = b = 8.334(2)$  Å and  $c = 7.843(2)$  Å. This lattice expansion is expected if less titanium substituted for zirconium on the Zr(2) site and suggests that there is a homogeneity range for this phase.

The sample was checked for superconductivity, but none was detected down to 6 K. Magnetic measurements show the sample is Pauli paramagnetic.

### Discussion

This new structure may usefully be compared to the  $\kappa$ -phases.<sup>16</sup>  $\kappa$ -phases crystallize in the hexagonal space group  $P6_3/mmc$ . This new phase crystallizes in the trigonal space group  $P\bar{3}m1$ . Figure 5 compares the metal framework in the structures of these two phases, viewed perpendicular to the  $[110]$  direction. The oxygen atoms are omitted in this figure. Figure 5a is similar to Figure 4, showing the icosahedral coordination of silicon (B) between the two layers of zirconium trigonal antiprisms (A). Figure 5b is a view of the  $\kappa$ -phase, which also contains parallel layers of trigonal antiprisms made up of the metal atoms, M, at the top and bottom of the figure (A). A horizontal mirror plane contains the interstitial atom, X, and one face of the trigonal antiprism. It can be noticed that the parallel layers are connected by a middle antiparallel layer (A'). The interstitial atom has a tricapped trigonal prismatic coordination. The new structure can be pictured as a distortion of the  $\kappa$ -phase, where the distortion consists of expanding one trigonal face of the trigonal prism, as indicated by the arrows in Figure 5b, and moving the atoms to a position corresponding to the Ni atoms in Figure 5a. The interstitial

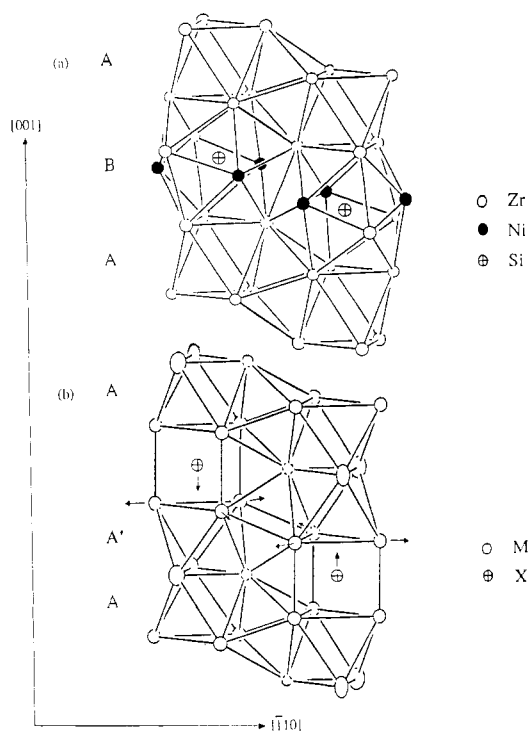


**Figure 5.** (a)  $\text{Zr}_6\text{Ni}_6\text{TiSiO}_2$ . (b)  $\kappa$ -phase. Arrows show direction of distortion leading to the new structure.

atom then moves into this expanded region. A compression along the  $c$  axis completes the distortion (a value of  $c/a = 0.97$ – $0.99$  is typical for the  $\kappa$ -phases, compared to  $c/a = 0.90$  for the new structure).

The  $\kappa$ -phases are an intriguing class of compounds, in which the metal framework provides a host to many different interstitial elements. The general formula for the  $\kappa$ -phase is  $\text{M}_9\text{M}'_4\text{X}$ , where  $\text{X} = \text{B}, \text{C}, \text{Si}, \text{Ge}, \text{P}, \text{As}, \text{S}, \text{Se}, \text{Fe}, \text{Co},$  or  $\text{Ni}$ . Apparently, the strength of the metal-metal interactions in the framework allows for the variability in  $\text{X}$ . A similar argument suggests that this new phase might also form with a variety of interstitial elements. The  $\kappa$ -phase and the new phase both have a metal/nonmetal ratio of 13:1, neglecting the oxygen. The difference between the two phases is the metals which make the framework. The  $\kappa$ -phase framework contains two transition metals, while this new phase has ternary framework with two early transition metals and a late transition metal. Continuing investigations will determine if this phase forms with other interstitial elements and if other metals will substitute in this framework.

**Acknowledgment.** The authors acknowledge the assistance of J. W. Andereggs for the XPS work, G. L. Schimek for the EDX analysis, and J. E. Ostenson for the magnetic measurements.

**Supplementary Material Available:** Anisotropic displacement parameters (1 page); listing of structure factor data (4 pages). Ordering information is given on any current masthead page.